First-principles study of the magnetic ground state and magnetization process of the kagome francisites $Cu_3Bi(SeO_3)_2O_2X$ (X=Cl, Br)

S. A. Nikolaev,[1,*] V. V. Mazurenko,[1] A. A. Tsirlin,[1,2,†] and V. G. Mazurenko[1]

[1]*Department of Theoretical Physics and Applied Mathematics, Ural Federal University, 620002 Yekaterinburg, Russia*

[2]*Experimental Physics VI, Center for Electronic Correlations and Magnetism, Institute of Physics, University of Augsburg, 86135 Augsburg, Germany*

(Received 16 March 2016; revised manuscript received 15 September 2016; published 12 October 2016)

We explore the magnetic behavior of the kagome francisites $Cu_3Bi(SeO_3)_2O_2X$ (X=Cl, Br) by using first-principles electronic structure calculations. To this end, we propose an approach based on the effective Hubbard model in the Wannier functions basis constructed on the level of local-density approximation. The ground-state spin configuration is determined by a mean-field Hartree-Fock solution of the Hubbard model both in zero magnetic field and in applied magnetic fields. Additionally, parameters of an effective spin Hamiltonian are obtained by taking into account hybridization effects and spin-orbit coupling. We show that only the former approach based on the Hartree-Fock approximation allows for a complete description of the anisotropic magnetization process. While our calculations confirm that the canted zero-field ground state arises from a competition between ferromagnetic nearest-neighbor and antiferromagnetic next-nearest-neighbor couplings in the kagome planes, weaker anisotropic terms are crucial for fixing spin directions and for the strong anisotropy of the magnetization. We show that the Hartree-Fock solution of an electronic Hamiltonian is a viable alternative to the analysis of effective spin Hamiltonians when magnetic ground states and their evolution in external field are concerned.

DOI: 10.1103/PhysRevB.94.144412

I. INTRODUCTION

The interest in novel frustrated magnetic compounds is continuously increasing because of the wide diversity of their crystal structures and magnetic configurations leading, in turn, to many interesting phenomena that may be relevant to different applications, such as spintronics [1,2]. For example, systems composed of $S = \frac{1}{2}$ spins on a two-dimensional kagome-type lattice are usually strongly frustrated due to competing exchange interactions that give rise to various exotic ground states and peculiar properties at finite temperatures and in applied magnetic fields [3].

Owing to difficulties in synthesizing inorganic compounds with a low-dimensional arrangement of transition-metal cations, one usually resorts to special strategies for their construction. For instance, inorganic polyanionic groups can be used as a spacer to form open volumes excluding bonding along one or two directions of the crystal structure. Ideal candidates for this purpose are stereochemically active lone-pair cations (Se^{+4} or Bi^{+3}), which are large enough to expand a crystal structure and form bonds only with oxygen ions [4,5]. Halogens are often used as well, because they prefer low coordination numbers and thus act as terminating species [6].

$Cu_3Bi(SeO_3)_2O_2X$ with X = Br and Cl, hereinafter referred to as CBSOOX, are geometrically frustrated layered compounds with noncollinear magnetic order [7]. They can be derived from the natural mineral francisite and crystallize in the orthorhombic $Pmmn$ structure [8]. This structure can be described as formed by copper(II)-oxygen layers with two nonequivalent copper sites, Cu1 and Cu2 of the site symmetries -1 and $mm2$, respectively, that build up a hexagonal network of CuO_4 square plaquettes linked together by Se^{+4} and Bi^{3+} ions with different out-of-plane oxygen bonding [Fig. 1(a)]. This geometry can be regarded as buckled kagome-type lattice.

Anisotropic magnetic properties of CBSOOX were studied by bulk magnetization measurements [8] and single-crystal neutron diffraction [7] that revealed the magnetic ordering transition around 27 K. In zero field, the magnetic ground state is formed by antiferromagnetically coupled ab layers, where magnetic moments on the Cu2 sites point along the $\boldsymbol{c}$ axis, whereas those on the Cu1 sites are canted from $\boldsymbol{c}$ towards $\boldsymbol{b}$, thus producing the net magnetic moment within each layer in the ab plane. These moments cancel out macroscopically because of the weakly antiferromagnetic interlayer coupling that can be overridden by a magnetic field $B_C \approx 0.8$ T applied along the $\boldsymbol{c}$ axis. External field triggers a metamagnetic transition, wherein magnetic moments in every second layer flip, and the net magnetic moment is formed macroscopically [7,9]. Qualitatively similar behavior was observed in CBSOOCl [10], although no details of its magnetic structure were reported.

Rousochatzakis *et al.* [11] used density-functional theory calculations to derive isotropic and anisotropic exchange couplings in kagome francisites. They constructed an effective spin Hamiltonian that was subsequently analyzed on the classical level and, for the isotropic part of the Hamiltonian, using the coupled cluster method, where quantum effects were included. According to Ref. [11], canted spin order in the ab plane of kagome francisites originates from the competition between ferromagnetic nearest-neighbor ($J_1 \simeq -70$ K) and antiferromagnetic next-nearest-neighbor ($J_2 \simeq 50$ K) interactions. The leading Dzyaloshinsky-Moriya component along the $\boldsymbol{a}$ direction (d_{1a} in the notation of Ref. [11]) restricts canted spins to the bc plane. However, their orientation within the bc plane and the alignment of the net magnetic

*saishi@inbox.ru

†altsirlin@gmail.com

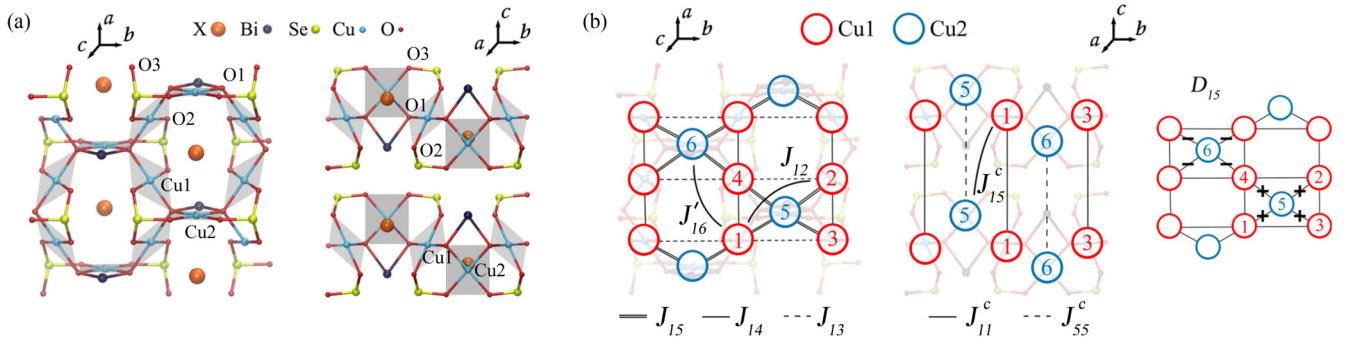

FIG. 1. (a) Crystal structure of CBSOOX: *ab* (left) and *bc* (right) projections; (b) schematic view of intraplane (left panel) and interplane (right panel) isotropic exchange parameters. Sites 1, 2, 3, 4 and 5, 6 stand for the Cu1 and Cu2 atoms, respectively. Equivalent bonds are shown by the same color. The sign of the a component of the anisotropic exchange coupling $\boldsymbol{D}_{15}$ is shown by + and −.

moment along the $\boldsymbol{c}$ direction could not be reproduced, and the anisotropic magnetization process was not described quantitatively.

Recent experimental studies revealed new unusual features of kagome francisites. These compounds exhibit field- and temperature-dependent microwave absorption over at least ten decades of frequency [12,13]. This effect can be used for microwave filtering [12] and calls for a microscopic description of the magnetization process. In the following, we will show how this description can be achieved. The novelty of our approach lies in the direct treatment of the electronic Hamiltonian, where all isotropic and anisotropic exchange couplings are included implicitly. We then use the same band structure to derive parameters of the effective spin Hamiltonian, and demonstrate salient differences between the modeling approaches based on the electronic and spin Hamiltonians.

II. CONSTRUCTION OF WANNIER FUNCTIONS

Electronic structure calculations have been performed in terms of the conventional local-density approximation (LDA) [14] and projected augmented wave [15] formalisms, as implemented in the Vienna *ab initio* simulation package [16]. Hopping parameters including spin-orbit coupling (LDA+SO) were calculated in the QUANTUM ESPRESSO package [17]. To take into account on-site Coulomb correlations between Cu $3d$ states, the LDA+U scheme has been employed [18]. In our studies, we adopt the experimental crystallographic data from Ref. [8] listed in Table I. The unit cell contains six copper atoms with fractional coordinates presented in Table I.

The LDA and LDA+SO band structures of CBSOOX are presented in Fig. 2(a). One of the most important features of the electronic structure is the presence of six bands located near the Fermi level and well separated from the rest of the spectrum. These states are formed by Cu $3d^{x^2-y^2}$ and O $2p$ states. The relevant Wannier functions [19] can be expressed as the following linear combinations:

$$W_1 = \alpha_1\phi^{x^2-y^2}_{\mathrm{Cu1}} + 2\beta_1\phi^{p}_{\mathrm{O1}} + 2\beta_2\phi^{p}_{\mathrm{O2}} + 2\gamma\phi_{\mathrm{Se}} \qquad (1)$$

and

$$W_2 = \alpha_2\phi^{x^2-y^2}_{\mathrm{Cu2}} + 2\beta_1\phi^{p}_{\mathrm{O1}} + 2\beta_3\phi^{p}_{\mathrm{O3}} \qquad (2)$$

for Cu1 and Cu2 sites, respectively, where contributions from bismuth and halogen orbitals are supposed to be negligible. The coefficients in Eqs. (1) and (2) are determined using magnetic moments obtained from LDA+U calculations for the ferromagnetic spin configuration. The values of α_i^2 are related to the magnetization of copper ions, whereas the coefficients for oxygen and selenium atomic orbitals can be found in the same way from their magnetic moments divided by the number of Wannier functions overlapping at these sites [20]. The resulting Wannier functions obtained from LDA calculations are presented in Fig. 2(b). Their structure is consistent with Eqs. (1) and (2).

For LDA+U calculations, we used the on-site Coulomb repulsion $U = 9$ eV and the intra-atomic exchange parameter $J = 1$ eV. These values are in the common range for copper-based compounds, as shown in Table II, and give quantitative agreement with the experiment. We found the energy gap of 2.9 eV, which is compatible with the green color of francisite crystals. The calculated magnetic moments used to estimate the expansion coefficients, Eqs. (1) and (2), are presented in Table III.

III. CONSTRUCTION OF THE HUBBARD MODEL

To describe electronic and magnetic properties of CBSOOX, we construct the following one-orbital Hubbard

TABLE I. Lattice constants and fractional coordinates of copper atoms of the $Pmmn$ CBSOOX crystal structure as reported in Ref. [8]. See Fig. 1(b) for details.

	$Cu_3Bi(SeO_3)_2O_2Cl$	$Cu_3Bi(SeO_3)_2O_2Br$
a (Å)	6.3540	6.3900
b (Å)	9.6350	9.6940
c (Å)	7.2330	7.2870
Cu1 1	(0.0,0.0,0.0)	(0.0,0.0,0.0)
2	$(\frac{1}{2},\frac{1}{2},0.0)$	$(\frac{1}{2},\frac{1}{2},0.0)$
3	$(0.0,\frac{1}{2},0.0)$	$(0.0,\frac{1}{2},0.0)$
4	$(\frac{1}{2},0.0,0.0)$	$(\frac{1}{2},0.0,0.0)$
Cu2 5	$(\frac{1}{4},\frac{1}{4},0.7920)$	$(\frac{1}{4},\frac{1}{4},0.7925)$
6	$(\frac{3}{4},\frac{3}{4},0.2080)$	$(\frac{3}{4},\frac{3}{4},0.2075)$

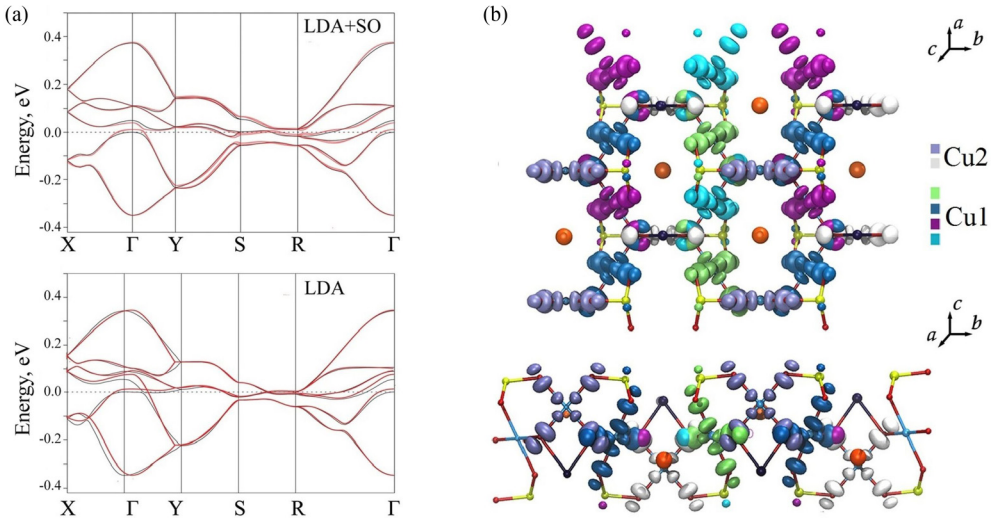

FIG. 2. (a) Bands located near the Fermi level as obtained from LDA+SO (up) and LDA (down) calculations for CBSOOBr. The red lines show the Wannier parametrization. The notation of k points is $X(\frac{1}{2},0,0)$, $\Gamma(0,0,0)$, $Y(0,\frac{1}{2},0)$, $S(\frac{1}{2},\frac{1}{2},0)$, and $R(\frac{1}{2},\frac{1}{2},\frac{1}{2})$ in reciprocal lattice units. (b) Wannier functions centered on copper atoms, as obtained from LDA calculations for CBSOOBr.

model [21]:

$$\hat{\mathcal{H}} = \sum_{\boldsymbol{R}\boldsymbol{R}',\sigma\sigma'} t^{\sigma\sigma'}_{\boldsymbol{R}\boldsymbol{R}'} \hat{a}^{\dagger}_{\boldsymbol{R}\sigma}\hat{a}_{\boldsymbol{R}'\sigma'} + \frac{1}{2}\sum_{\boldsymbol{R},\sigma\sigma'} U_{\boldsymbol{R}}\, \hat{a}^{\dagger}_{\boldsymbol{R}\sigma}\hat{a}^{\dagger}_{\boldsymbol{R}\sigma'}\hat{a}_{\boldsymbol{R}\sigma'}\hat{a}_{\boldsymbol{R}\sigma} + \frac{1}{2}\sum_{\boldsymbol{R}\boldsymbol{R}',\sigma\sigma'} J^{H}_{\boldsymbol{R}\boldsymbol{R}'}\, \hat{a}^{\dagger}_{\boldsymbol{R}\sigma}\hat{a}^{\dagger}_{\boldsymbol{R}'\sigma'}\hat{a}_{\boldsymbol{R}\sigma'}\hat{a}_{\boldsymbol{R}'\sigma}, \quad (3)$$

where $\hat{a}^{\dagger}_{\boldsymbol{R}\sigma}$ ($\hat{a}_{\boldsymbol{R}\sigma}$) creates (annihilates) an electron of spin σ at site $\boldsymbol{R}$, $U_{\boldsymbol{R}}$ and $J^{H}_{\boldsymbol{R}\boldsymbol{R}'}$ are the local Coulomb and nonlocal exchange interactions, respectively, and $t^{\sigma\sigma'}_{\boldsymbol{R}\boldsymbol{R}'}$ is the hopping matrix element corresponding to the LDA+SO band structure.

The hopping integrals were calculated from a Wannier parametrization of the LDA and LDA+SO band structures [22]. Their values for the interaction paths shown in Fig. 1(b) are presented in Table IV, while the rest of the hopping integrals can be obtained by applying symmetry operations of the $Pmmn$ space group. The LDA-based hopping parameters and real parts of the LDA+SO-based hoppings match quite well. The LDA+SO hopping integrals additionally contain large imaginary nondiagonal elements due to spin-orbit coupling. As we show below, these imaginary components are responsible for anisotropic exchange interactions.

TABLE II. List of the on-site Coulomb interaction U and intra-atomic exchange interaction J for the Cu $3d$ shell used for LDA+U calculations of Cu-based compounds.

	U (eV)	J (eV)
This work	9.0	1.0
$Cu_3Bi(SeO_3)_2O_2Br$, Ref. [11]	9.5	1.0
$LiCu_2O_2$, Ref. [20]	10.0	1.0
$SrCu_2(BO_3)_2$, Ref. [23]	9.4	1.0
$La_4Ba_2Cu_2O_{10}$, Ref. [24]	6.7	0.7
$CdCu_2(BO_3)$, Ref. [25]	9.5	1.0

The on-site Coulomb and nonlocal exchange interaction parameters are defined in the atomiclike basis using atomic decomposition of individual Wannier orbitals, Eqs. (1) and (2) [20,23]. This way, we obtain $U_{\boldsymbol{R}} \approx \alpha^4 U = 5.09$ eV in agreement with the effective Hubbard U calculated within the constrained random phase approximation: for example, $U_{\text{eff}} = 5.5$ and 3.65 eV were obtained for copper metal [26] and La_2CuO_4 [27], respectively.

The exchange parameter of Eq. (3) is defined as follows [20,23]:

$$J^{H}_{\boldsymbol{R}\boldsymbol{R}'} = \beta^4 J^{p,\mathrm{O}} + \gamma^4 J^{p,\mathrm{Se}}, \quad (4)$$

where $J^{p,\mathrm{O}}$ and $J^{p,\mathrm{Se}}$ are the intra-atomic exchange interactions for oxygen and selenium ions, respectively. Their values can be estimated from LDA+U calculations as the shift of band centers for the majority $C^{\uparrow}$ and minority $C^{\downarrow}$ spin components, $J^{p,I} = (C^{\uparrow}_I - C^{\downarrow}_I)/M_I$, where M_I is the magnetic moment of the corresponding atom [28]. We find $J^{p,\mathrm{O}} = 1.5$ eV and $J^{p,\mathrm{Se}} = 0.9$ eV. Our estimate of $J^{p,\mathrm{O}}$ is consistent with the values of 1.6 eV [28] and 1.2 eV [29] reported in the previous literature. The resulting $J^{H}_{\boldsymbol{R}\boldsymbol{R}'} = 4.26$ meV is further justified *a posteriori* by good agreement between nearest-neighbor ferromagnetic exchange couplings obtained in our work (Table V) and in the direct LDA+U+SO calculation of Ref. [11]. Moreover, this value

TABLE III. Magnetic moments (in μ_B) and corresponding expansion coefficients in Eqs. (1) and (2) obtained from LDA+U calculations for the ferromagnetic configuration.

X	m_{Cu1} (α^4_1)	m_{Cu2} (α^4_2)	m_{O1} (β^4_1)	m_{O2} (β^4_2)	m_{O3} (β^4_3)	m_{Se} (γ^4)	m_{Bi}
Cl	0.757	0.746	0.160	0.046	0.047	0.018	0.006
	(0.573)	(0.557)	(0.0028)	(0.0022)	(0.0022)	(0.0003)	
Br	0.758	0.750	0.158	0.044	0.042	0.020	0.006
	(0.575)	(0.563)	(0.0028)	(0.0019)	(0.0018)	(0.0004)	

TABLE IV. Hopping integrals $t_{ij}^{\sigma\sigma'}$ (in meV) as obtained from LDA+SO and LDA calculations. The leading couplings are bold-faced. The corresponding interatomic distances are given by d. The superscripts a, b, and c denote next-nearest neighbors along the corresponding crystallographic directions. Indices 1, 2, 3, 4 and 5, 6 represent the Cu1 and Cu2 sites, respectively. See Fig. 1(b) for details.

	$Cu_3Bi(SeO_3)_2O_2Cl$			$Cu_3Bi(SeO_3)_2O_2Br$		
	d (Å)	LDA	LDA+SO	d (Å)	LDA	LDA+SO
Intraplane						
$\boldsymbol{t_{13}}$	4.817	**−78.9**	$\begin{pmatrix} \mathbf{-78.4-3.9}i & \mathbf{-2.6}i \\ \mathbf{-2.6}i & \mathbf{-78.4+3.9}i \end{pmatrix}$	4.846	**−72.4**	$\begin{pmatrix} \mathbf{-71.3-2.4}i & \mathbf{-1.1}i \\ \mathbf{-1.1}i & \mathbf{-71.3+2.4}i \end{pmatrix}$
$\boldsymbol{t_{14}}$	3.177	**−0.1**	$\begin{pmatrix} \mathbf{-1.2-5.6}i & \mathbf{9.3} \\ \mathbf{-9.3} & \mathbf{-1.2+5.6}i \end{pmatrix}$	3.195	**−8.1**	$\begin{pmatrix} \mathbf{-10.2-19.9}i & \mathbf{17.6} \\ \mathbf{-17.6} & \mathbf{-10.2+19.9}i \end{pmatrix}$
$\boldsymbol{t_{15}}$	3.254	**−46.4**	$\begin{pmatrix} \mathbf{-45.8-12.9}i & \mathbf{10.1-25.1}i \\ \mathbf{-10.1-25.1}i & \mathbf{-45.8+12.9}i \end{pmatrix}$	3.273	**−33.1**	$\begin{pmatrix} \mathbf{-32.7-8.3}i & \mathbf{15.8-32}i \\ \mathbf{-15.8-32}i & \mathbf{-32.7+8.3}i \end{pmatrix}$
t_{12}	5.771	26.4	$\begin{pmatrix} 24.7-2.1i & 4.8 \\ -4.8 & 24.7+2.1i \end{pmatrix}$	5.805	28.1	$\begin{pmatrix} 25.0-3.3i & 7.1-0.8i \\ -7.1-0.8i & 25.0+3.3i \end{pmatrix}$
t_{11}^b	6.354	−5.9	$\begin{pmatrix} -3.1-0.5i & -2.1i \\ -2.1i & -3.1+0.5i \end{pmatrix}$	6.390	−11.4	$\begin{pmatrix} -8.2-1.1i & -3.0i \\ -3.0i & -8.2+1.1i \end{pmatrix}$
t_{55}^a	9.639	23.5	$\begin{pmatrix} 17.2-0.9i & -1.4-0.3i \\ 1.4-0.3i & 17.2+0.9i \end{pmatrix}$	9.693	30.6	$\begin{pmatrix} 19.1-0.7i & -2.8-0.4i \\ 2.8-0.4i & 19.1+0.7i \end{pmatrix}$
t_{16}'	5.548	−35.2	$\begin{pmatrix} -33.8-1.6i & 1.4-0.6i \\ -1.4-0.6i & -33.8+1.6i \end{pmatrix}$	5.579	−31.5	$\begin{pmatrix} -29.3+1.3i & -1.6+0.7i \\ 1.6+0.7i & -29.3-1.3i \end{pmatrix}$
Interplane						
t_{11}^c	7.233	10.8	$\begin{pmatrix} 8.2+0.1i & -0.2+0.2i \\ 0.2+0.2i & 8.2-0.1i \end{pmatrix}$	7.287	7.5	$\begin{pmatrix} 4.4 & -0.3+0.1i \\ 0.3+0.1i & 4.4 \end{pmatrix}$
t_{55}^c	7.233	22.5	$\begin{pmatrix} 19.8-0.1i & -0.1 \\ 0.1 & 19.8+0.1i \end{pmatrix}$	7.287	17.3	$\begin{pmatrix} 14.5-0.1i & -0.1 \\ 0.1 & 14.5+0.1i \end{pmatrix}$
t_{15}^c	6.426	9.3	$\begin{pmatrix} 6.3 & 0.0 \\ 0.0 & 6.3 \end{pmatrix}$	6.463	8.7	$\begin{pmatrix} 6.9 & 0.0 \\ 0.0 & 6.9 \end{pmatrix}$

of the $J^H_{\boldsymbol{RR'}}$ parameter delivers a quantitative description of the experimental magnetic structure and magnetization process (see Sec. V below).

The Hubbard model constructed in Eq. (3) can be solved directly. Alternatively, one can follow the strategy of Ref. [11] and extract parameters of the spin Hamiltonian that is further solved on the classical level or using advanced numerical techniques that take into account quantum effects. In the following, we will follow both approaches and demonstrate that the second approach suffers from a truncation problem, because only a limited number of the anisotropy terms can be included in the spin Hamiltonian. On the other hand, the first approach relying on a direct solution of the Hubbard Hamiltonian is free from this problem and, therefore, provides quantitative description of the magnetic properties in francisites.

IV. MICROSCOPIC ANALYSIS OF MAGNETIC INTERACTIONS

In the limit $t \ll U$ that holds for francisites, one can construct a Heisenberg-type model by using the superexchange theory proposed by Anderson [30,31]:

$$H = \sum_{\boldsymbol{RR'}} J_{\boldsymbol{RR'}} \hat{\boldsymbol{S}}_{\boldsymbol{R}} \hat{\boldsymbol{S}}_{\boldsymbol{R'}} + \sum_{\boldsymbol{RR'}} \boldsymbol{D}_{\boldsymbol{RR'}} [\hat{\boldsymbol{S}}_{\boldsymbol{R}} \times \hat{\boldsymbol{S}}_{\boldsymbol{R'}}], \qquad (5)$$

where $J_{\boldsymbol{RR'}}$ and $\boldsymbol{D}_{\boldsymbol{RR'}}$ are the isotropic and anisotropic (Dzyaloshinsky-Moriya) exchange interactions between the $\boldsymbol{R}$th and $\boldsymbol{R'}$th sites, respectively.

In terms of the Hubbard model parameters, Eq. (3), the isotropic exchange interaction is expressed in the following form:

$$J_{\boldsymbol{RR'}} = \frac{2}{U_{\boldsymbol{R}}} \mathrm{Tr}\{\hat{t}_{\boldsymbol{R'R}} \hat{t}_{\boldsymbol{RR'}}\} - 2J^H_{\boldsymbol{RR'}}. \qquad (6)$$

The first term in Eq. (6) is the kinetic Anderson's exchange interaction, while the second one is the ferromagnetic exchange arising from the overlap between the neighboring Wannier functions [20]. As seen from Figs. 1(b) and 2(b), it has a nonzero value for the 1–4 and 1–5 copper bonds.

The resulting isotropic exchange parameters calculated using Eq. (6) from the LDA+SO band structure are presented in Table V. We find a strong intraplane ferromagnetic (FM) coupling defined by the nearest-neighbor Cu1-Cu2 and Cu1-Cu1 interactions, J_{15} and J_{14}, respectively. The dominant intraplane antiferromagnetic (AFM) exchange interaction J_{13} is found between the neighboring Cu1 sites, for which the corresponding magnetic orbitals do not overlap on the oxygen atoms. This coupling is about two times smaller than the FM one.

Our results are in good agreement with the previous theoretical analysis [11] that reported $J_{13} = 4.74$ (5.08) meV, $J_{14} = -6.54$ (−6.46) meV, and $J_{15} = -5.68$ (−5.77) meV for $X =$ Cl (Br). The copper atoms in adjacent layers are coupled antiferromagnetically, and the interplane interaction is essentially weak (about 10–20 times smaller than the corresponding intraplane interactions). The isotropic exchange parameters are very similar for $X =$ Cl and Br, which implies a

TABLE V. Isotropic J_{ij} and anisotropic $\boldsymbol{D}_{ij}$ exchange parameters (in meV) between copper $d^{x^2-y^2}$ orbitals as obtained from LDA+SO calculations. The leading couplings are bold-faced. The superscripts a, b, and c denote next-nearest neighbors along the corresponding crystallographic directions. Indices 1, 2, 3, 4 and 5, 6 represent the Cu1 and Cu2 sites, respectively. See Fig. 1(b) for details.

	$Cu_3Bi(SeO_3)_2O_2Cl$	$Cu_3Bi(SeO_3)_2O_2Br$
$\boldsymbol{J_{13}}$	**4.84**	**4.01**
$\boldsymbol{J_{14}}$	**−8.43**	**−8.29**
$\boldsymbol{J_{15}}$	**−6.17**	**−7.43**
J_{12}	0.50	0.54
J^b_{11}	0.01	0.06
J^a_{55}	0.23	0.29
J'_{16}	0.90	0.68
J^c_{11}	0.05	0.02
J^c_{55}	0.31	0.17
J^c_{15}	0.03	0.03
$\boldsymbol{D_{13}}$	(**0.18**, **0.0**, **0.27**)	(**0.07**, **0.0**, **0.15**)
$\boldsymbol{D_{14}}$	(**0.0**, **0.10**, **0.06**)	(**0.0**, **0.16**, **0.18**)
$\boldsymbol{D_{15}}$	(**1.02**, **0.41**, **0.33**)	(**0.93**, **0.46**, **0.24**)

small contribution of halogen's p states to the localized bands near the Fermi level.

Dzyaloshinskii-Moriya (DM) interactions. Anisotropic exchange parameters can be derived by extending the superexchange theory to the relativistic case with spin-orbit coupling. They have the following form [30,32]:

$$\boldsymbol{D}_{\boldsymbol{RR'}} = -\frac{i}{U_{\boldsymbol{R}}}[\mathrm{Tr}\{\hat{t}_{\boldsymbol{R'R}}\}\mathrm{Tr}\{\hat{t}_{\boldsymbol{RR'}}\boldsymbol{\sigma}\} - \mathrm{Tr}\{\hat{t}_{\boldsymbol{RR'}}\}\mathrm{Tr}\{\hat{t}_{\boldsymbol{R'R}}\boldsymbol{\sigma}\}], \tag{7}$$

where $\boldsymbol{\sigma}$ is a vector of the Pauli matrices. The values of anisotropic exchange parameters are presented in Table V. The dominant anisotropic exchange coupling is found between the atoms 1 and 5 ($\boldsymbol{D}_{15}$), and its component along the $\boldsymbol{a}$ axis is by far the largest among the DM couplings. The value of $\boldsymbol{D}_{15}$ is mostly determined by the relatively large hopping parameters t_{15}. Moreover, the a component of $\boldsymbol{D}_{15}$ has different orientations in two adjacent hexagonal networks of the same ab layer [Fig. 1(b)], and is responsible for the stabilization of the canted magnetic order [11]. It also puts spins in the bc plane, but does not choose spin directions within this plane [11].

Our results for the exchange parameters obtained within Moriya's microscopic theory [Eq. (5)] are in good agreement with those estimated from LDA+U+SO total energies [11]. They also follow symmetry constraints imposed by the crystal structure. The $\boldsymbol{D}_{13}$ and $\boldsymbol{D}_{14}$ vectors lie in the ac and bc planes, respectively, because these exchange bonds are crossed by the mirror planes. On the other hand, $\boldsymbol{D}_{15}$ has an arbitrary direction, because it pertains to the exchange bond between the atoms Cu1 and Cu2, which are not related by symmetry.

V. HARTREE-FOCK SOLUTION OF THE ELECTRONIC HAMILTONIAN

As an alternative to the parametrization of the spin Hamiltonian, Eq. (5), we consider direct solution of the effective Hubbard model, Eq. (3), both in zero field and in applied magnetic fields, which are modeled by including the Zeeman term:

$$\hat{\mathcal{H}}^Z = \sum_{\boldsymbol{R}} \mu_B g_s \boldsymbol{B}\cdot\hat{\boldsymbol{S}}_{\boldsymbol{R}}, \tag{8}$$

where $\hat{\boldsymbol{S}}_{\boldsymbol{R}} = \frac{1}{2}\sum_{\sigma\sigma'}\hat{a}_{\boldsymbol{R}\sigma}\boldsymbol{\sigma}^{\sigma\sigma'}\hat{a}^{\dagger}_{\boldsymbol{R}\sigma'}$ stands for the localized magnetic moment, μ_B is the Bohr magneton, and $g_s \approx 2.0$ is the gyromagnetic ratio. Generally, the Zeeman term describes the full magnetic moment interacting with an external field. However, since the one-orbital model is employed, the orbital magnetic moment is neglected and we consider only its spin counterpart.

The Hubbard Hamiltonian is solved in the Hartree-Fock approximation. Although mean-field in nature, this approximation should capture all relevant physics of kagome francisites, where both charge and spin fluctuations are weak. Indeed, the insulating state of francisites with a sizable band gap of 2.9 eV is clearly established by LSDA+U calculations. This is also obvious from the light-green color of francisite crystals and implies that charge fluctuations are absent. Spin fluctuations play a minor role as well, because experimental ordered moments are about $0.90\mu_B$ in zero field and increase up to $0.99\mu_B$ in the applied field of 1 T [7], thus approaching the full moment of $1.0\mu_B$ for the spin-$\frac{1}{2}$ Cu^{2+} ion.

By using the mean-field Hartree-Fock approximation, the one-orbital Hubbard model can be solved as follows [33]:

$$\left(\hat{t}_{\mathbf{k}} + \hat{\mathcal{U}} + \hat{\mathcal{V}}^H + \hat{\mathcal{V}}^H_{\mathbf{k}}\right)|\varphi_{\mathbf{k}}\rangle = \varepsilon_{\mathbf{k}}|\varphi_{\mathbf{k}}\rangle, \tag{9}$$

where $\hat{t}_{\mathbf{k}} = \sum_{\boldsymbol{RR'}}\hat{t}_{\boldsymbol{RR'}}e^{-i\mathbf{k}(\boldsymbol{R}-\boldsymbol{R'})}$ is the Fourier image of the LDA+SO hopping parameters, $\varepsilon_{\mathbf{k}}$ and $|\varphi_{\mathbf{k}}\rangle$ are eigenvalues and eigenvectors in the basis of Wannier functions, respectively, $\hat{\mathcal{U}} = \sum_{\boldsymbol{R}}\hat{\mathcal{U}}_{\boldsymbol{R}}$, $\hat{\mathcal{V}}^H = \sum_{\boldsymbol{R}}\hat{\mathcal{V}}^H_{\boldsymbol{R}}$, and $\hat{\mathcal{V}}^H_k = \sum_{\boldsymbol{RR'}}\hat{\mathcal{V}}^H_{k,\boldsymbol{RR'}}$ are the Hartree-Fock potentials, where the first term includes the on-site Coulomb and Zeeman interactions:

$$\hat{\mathcal{U}}_{\boldsymbol{R}} = \begin{pmatrix} U_{\boldsymbol{R}}n^{\downarrow\downarrow}_{\boldsymbol{R}} + \mu_B B_z & -U_{\boldsymbol{R}}n^{\downarrow\uparrow}_{\boldsymbol{R}} + \mu_B(B_x - iB_y) \\ -U_{\boldsymbol{R}}n^{\uparrow\downarrow}_{\boldsymbol{R}} + \mu_B(B_x + iB_y) & U_{\boldsymbol{R}}n^{\uparrow\uparrow}_{\boldsymbol{R}} - \mu_B B_z \end{pmatrix}, \tag{10}$$

while the other two terms originate from the nonlocal exchange coupling:

$$\hat{\mathcal{V}}^H_{\boldsymbol{R}} = -\sum_{\boldsymbol{R'}} J^H_{\boldsymbol{RR'}}\begin{pmatrix} n^{\uparrow\uparrow}_{\boldsymbol{R'}} & n^{\downarrow\uparrow}_{\boldsymbol{R'}} \\ n^{\uparrow\downarrow}_{\boldsymbol{R'}} & n^{\downarrow\downarrow}_{\boldsymbol{R'}} \end{pmatrix} \tag{11}$$

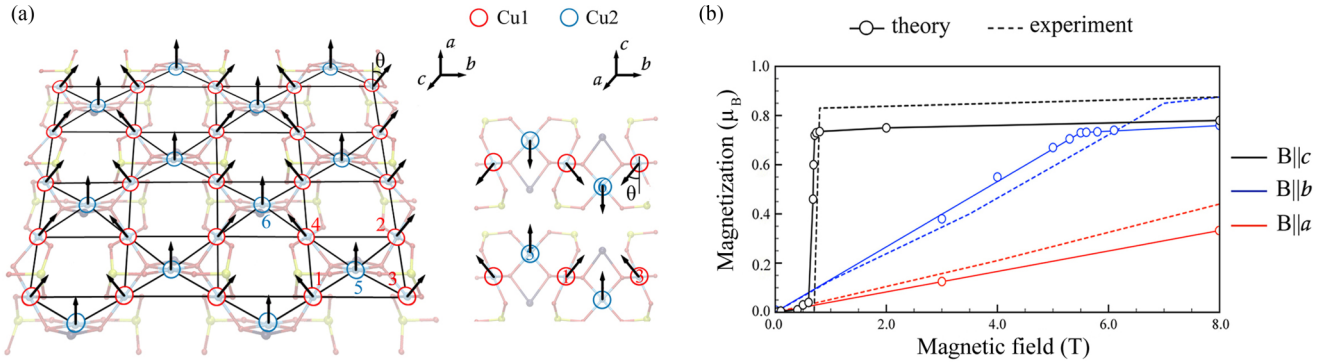

FIG. 3. (a) Magnetic lattice as obtained from the mean-field Hartree-Fock approximation at zero applied magnetic field. Sites 1, 2, 3, 4 and 5, 6 stand for the Cu1 and Cu2 atoms, respectively. (b) Total magnetization per site in CBSOOBr for three different directions of magnetic field $\boldsymbol{B}$ and their comparison with experimental data [7].

and

$$\hat{\mathcal{V}}^{H}_{\mathbf{k},\boldsymbol{RR'}} = J^{H}_{\boldsymbol{RR'}} e^{i\mathbf{k}(\boldsymbol{R}-\boldsymbol{R'})} \begin{pmatrix} n^{\uparrow\uparrow}_{\boldsymbol{RR'}} + n^{\downarrow\downarrow}_{\boldsymbol{RR'}} & 0 \\ 0 & n^{\uparrow\uparrow}_{\boldsymbol{RR'}} + n^{\downarrow\downarrow}_{\boldsymbol{RR'}} \end{pmatrix}, \tag{12}$$

where the on-site and intersite density matrices are defined as $\hat{n}_{\boldsymbol{R}} = \sum_k |\varphi_{\mathbf{k}}\rangle\langle\varphi_{\mathbf{k}}|$ and $\hat{n}_{\boldsymbol{RR'}} = \sum_k |\varphi_{\mathbf{k}}\rangle\langle\varphi_{\mathbf{k}}| e^{-i\mathbf{k}(\boldsymbol{R}-\boldsymbol{R'})}$, respectively. Iterative solution of the Hartree-Fock equations is obtained self-consistently with respect to the total energy:

$$E_{\mathrm{HF}} = \sum_{\mathbf{k}}^{occ} \varepsilon_{\mathbf{k}} - \frac{1}{2}\sum_{\boldsymbol{R}} \mathrm{Tr}[\hat{\mathcal{U}}_{\boldsymbol{R}}\hat{n}_{\boldsymbol{R}}] - \frac{1}{2}\sum_{\boldsymbol{R}} \mathrm{Tr}\big[\hat{\mathcal{V}}^{H}_{\boldsymbol{R}}\hat{n}_{\boldsymbol{R}}\big] - \frac{1}{2}\sum_{\boldsymbol{RR'}} J^{H}_{\boldsymbol{RR'}}\tilde{n}_{\boldsymbol{RR'}}\tilde{n}_{\boldsymbol{R'R}}, \tag{13}$$

where $\tilde{n}_{\boldsymbol{RR'}} = n^{\uparrow\uparrow}_{\boldsymbol{RR'}} + n^{\downarrow\downarrow}_{\boldsymbol{RR'}}$, and irreducible representations of the $Pmmn$ space group [7] are chosen as starting spin configurations. In our calculations, we use the LDA+SO hopping parameters presented in Table IV, the effective on-site Coulomb interaction $U_{\boldsymbol{R}} = 5.09$ eV and nonlocal exchange interaction $J^{H}_{\boldsymbol{RR'}} = 4.46$ meV.

In the absence of magnetic field, we find a canted order in the ab plane and antiferromagnetic stacking of these ferrimagnetic layers [Fig. 3(a)]. Magnetic moments on the Cu2 sites are strictly parallel to the $\boldsymbol{c}$ axis, while magnetic moments on the Cu1 sites alternate from this parallel direction towards the $\boldsymbol{b}$ axis and form canted magnetic texture with the bc angles $\theta = 50.1^\circ$ and 53.8° for $X =$ Cl and Br, respectively. This result is in good agreement with the experimental [7] and theoretical [11] values of the canting angle θ for $X =$ Br, 51.6° and 52.1°, respectively. Moreover, we obtain the Cu2 moment directed along the $\boldsymbol{c}$ axis purely from *ab initio*, which is different from Ref. [11], where an additional *ad hoc* assumption for the b and c components of $\boldsymbol{D_{15}}$ was required.

The magnetic moments for $X =$ Cl and Br are $\mathbf{m}_{\mathrm{Cu1}} = (0.01, 0.77, 0.64)\mu_B$ and $\mathbf{m}_{\mathrm{Cu2}} = (0.0, 0.0, 1.0)\mu_B$, and $\mathbf{m}_{\mathrm{Cu1}} = (0.0, 0.81, 0.59)\mu_B$ and $\mathbf{m}_{\mathrm{Cu2}} = (0.0, 0.0, 1.0)\mu_B$, respectively. Their directions are close to those obtained from the neutron diffraction measurements [7] for $X =$ Br, $\mathbf{m}_{\mathrm{Cu1}} = (0.0, 0.72, 0.57)\mu_B$ and $\mathbf{m}_{\mathrm{Cu2}} = (0.0, 0.0, 0.90)\mu_B$. On the other hand, quantum renormalization of the magnetic moments (reduction from $1.0\mu_B$ to $\sim 0.9\mu_B$ due to quantum fluctuations [11]) is not taken into account because of the mean-field nature of the Hartree-Fock approximation.

By applying symmetry operations of the $Pmmn$ space group, it follows that the magnetic ground state corresponds to the Γ_3 representation for both Cu sites. This representation allows for an additional canting out of the bc plane, and according to Ref. [11], this canting should be indeed present in kagome francisites, although it has not been detected in the experiment. Indeed, our zero-field ground state derived from the Hartree-Fock solution of the electronic Hamiltonian features a weak out-of-plane canting $\gamma = 0.8^\circ$ and 0.4° for $X =$ Cl and Br, respectively. The out-of-plane canting involves only the Cu1 spins and is much smaller compared to the in-plane canting.

In the case of the magnetic field $\boldsymbol{B}\|\boldsymbol{c}$, the zero-field AFM ground state becomes unstable and gives way to a high-field ferrimagnetic state with the critical field $\boldsymbol{B}_C = 0.87$ and 0.74 T for $X =$ Cl and Br, respectively [Fig. 3(b)], in agreement with the experimental value of ~ 0.8 T [7]. Since the AFM components are still present, we do not observe a full saturation to the FM state.

For the magnetic fields along the $\boldsymbol{a}$ and $\boldsymbol{b}$ axes, no metamagnetic transitions are observed, and the magnetic moments change continuously in each layer. In the case of $\boldsymbol{B}\|\boldsymbol{a}$, which acts against the leading a component of $\boldsymbol{D}_{15}$ and turns the magnetic moments out of the bc plane, we find an almost linear increase of the magnetization up to ~ 17.0 T and ~ 16.0 T for $X =$ Cl and Br, respectively, that is close to the (extrapolated) experimental value of ~ 15.0 T for $X =$ Br [7]. For $\boldsymbol{B}\|\boldsymbol{b}$, which changes the direction of the net moment without taking spins out of the bc plane, the magnetization increases faster. Net moments of individual layers are polarized at ~ 5.8 T and ~ 5.5 T for $X =$ Cl and Br, respectively, which is close to the experimental value of ~ 7.0 T for $X =$ Br [7]. The smaller slope of the magnetization with respect to the magnetic field $\boldsymbol{B}\|\boldsymbol{a}$ is a result of the dominant a component of $\boldsymbol{D}_{15}$. Altogether, we achieve a decent quantitative description of the anisotropic magnetization process of kagome francisites.

TABLE VI. Experimental quantities and their predictions based on LDA+SO, LDA+U+SO, and Hartree-Fock (HF) calculations: in-plane canting angle θ in the bc plane, out-of-plane canting angle γ for Cu1 spins, slopes of the magnetization curves κ_a and κ_c for $\boldsymbol{B}\|\boldsymbol{a}$ and $\boldsymbol{B}\|\boldsymbol{c}$, respectively, and the work (per site) W_b done by the magnetic field $\boldsymbol{B}\|\boldsymbol{b}$ when spins are polarized.

		θ (deg)	γ (deg)	κ_a (μ_B/T)	κ_c (μ_B/T)	W_b (μ_BT)
Br	LDA+SO	38.5	1.3	0.24	0.0082	0.076
	HF	53.8	0.4	0.045	0.0077	2.0
	LDA+U+SO [11]	52.1	0.7	0.16	0.0060	0.2
	Experiment [7]	51.6	–	0.066	0.0074	2.9
Cl	LDA+SO	51.4	1.0	0.15	0.0073	0.046
	HF	50.1	0.8	0.044	0.0061	2.2

VI. ELECTRONIC VS SPIN HAMILTONIANS

We are now in a position to compare our Hartree-Fock solution of the electronic Hamiltonian with the effective spin Hamiltonian obtained from the *same* LDA+SO band structure. To this end, we use several characteristic parameters derived in Ref. [11]. The primary canting angle θ and the out-of-plane canting angle γ are given by

$$J_{13}\sin 2\theta + J_{15}\sin\theta + D^a_{15}\cos\theta - D^a_{13}\cos 2\theta = 0 \quad (14)$$

and

$$\gamma = \frac{-D^b_{15} - D^b_{14}\cos\theta}{2J_{14} + J_{15}\sec\theta + D^a_{13}\tan\theta}. \quad (15)$$

The slopes of the magnetization curves for $\boldsymbol{B}\|\boldsymbol{a}$ and $\boldsymbol{B}\|\boldsymbol{c}$ are given by κ_a and κ_c, as follows:

$$\kappa_a = \frac{(g\mu_B)^2}{12}\frac{J_{15}(1+2\cos\theta)^2\csc\theta + D^a_{13} - 4D^a_{15}\cos\theta}{D^a_{15}\left(J_{15} + D^a_{13}\sin\theta\right) - J_{15}D^a_{13}\cos\theta}, \quad (16)$$

$$\kappa_c = \frac{(g\mu_B)^2/3}{2J_{13} + \left[D^a_{15} - D^a_{13}\cos\theta(1+2\sin^2\theta)\right]/\sin^3\theta}. \quad (17)$$

Finally, the slope of the magnetization curve for $\boldsymbol{B}\|\boldsymbol{b}$ is defined by the work W_b required to polarize spins along the field:

$$W_b = \frac{1}{3}\frac{\left(D^b_{15} + D^b_{14}\cos\theta\right)^2}{-2J_{14} + 2J_{13} + D^a_{15}\csc\theta - D^a_{13}\cot\theta}. \quad (18)$$

In Table VI, we list the experimental values of these parameters along with the results of Ref. [11] for $X = \mathrm{Br}$, where parameters of the spin Hamiltonian are obtained from LDA+U+SO calculations.

The values based on the spin Hamiltonian from LDA+SO and LDA+U+SO calculations ($X = \mathrm{Br}$) are qualitatively very similar, while minor quantitative differences can be traced back to different band-structure codes. The most tangible discrepancy is seen for the primary canting angle θ, where LDA+SO underestimates the canting because of the overestimated ferromagnetic couplings J_{14} and J_{15}. This overestimate is likely related to the approximate nature of Eq. (4) for non-90° ferromagnetic superexchange.

The Hartree-Fock solution of the electronic Hamiltonian mitigates the problem of the ferromagnetic superexchange and results in the realistic value of θ. Even more importantly, this solution largely improves the description of the magnetization curves, where, for example, LDA+SO and LDA+U+SO underestimate W_b by an order of magnitude. The Hartree-Fock solution correctly puts Cu2 spins (and thus the net magnetic moment) along the $\boldsymbol{c}$ axis, which is not expected from the spin Hamiltonian, where both b and c components of D_{15} (d_{1b} and d_{1c} in the notation of Ref. [11]) are clearly non-negligible suggesting a tilted direction of the net magnetic moment in the bc plane.

VII. SUMMARY AND CONCLUSIONS

We have shown that the spin Hamiltonian approach has its limitations in describing magnetic anisotropy of kagome francisites. Deficiencies of this approach are related to the fact that only the leading isotropic and anisotropic exchange couplings could be included in the theoretical analysis of Ref. [11]. For example, symmetric components of the anisotropy, albeit weak, were neglected, although they can also affect spin directions and induce peculiarities of the magnetization process. However, in a complex system like francisites, inclusion of the symmetric anisotropy renders the spin Hamiltonian cumbersome and makes the whole problem intractable for both analytical and numerical methods. In this case, the Hartree-Fock mean-field approximation for the electronic Hamiltonian provides a viable alternative that delivers the ground-state magnetic configuration both in zero and applied magnetic fields, so that the magnetization process can be modeled *ab initio*.

Our approach also has its limitations. Effects of thermal fluctuations are not included and only zero-temperature behavior is analyzed, while at zero temperature effects of quantum fluctuations are largely neglected. These effects do not compromise our analysis of francisites, because quantum fluctuations are weak in these systems, and experimental ordered moments are close to the spin-only value of $1.0\mu_B$ [7]. In complex spin systems, the effects of thermal and quantum fluctuations are usually incorporated on the level of spin Hamiltonians. Therefore, these two approaches based on the spin and electronic Hamiltonians are complimentary. Together they provide a complete microscopic scenario of a magnetic material.

ACKNOWLEDGMENTS

We are grateful to Ioannis Rousochatzakis for his fruitful comments about the manuscript. The work was supported by the grant program of the Russian Science Foundation 14-12-00306.

[1] D. P. Landau and K. Binder, Phys. Rev. B **24**, 1391 (1981).
[2] S. A. Wold, D. D. Awschalom, R. A. Buhrman, J. M. Daughton, S. von Molnar, M. L. Roukes, A. Y. Chtchelkanova, and D. M. Treger, Science **294**, 1488 (2001).
[3] L. Balents, Nature (London) **464**, 199 (2010).
[4] J. Galy, G. Meunier, S. Andersson, and A. Åström, J. Solid State Chem. **13**, 142 (1975).
[5] M. Johnsson, K. Törnroos, F. Mila, and P. Millet, Chem. Matter **12**, 2853 (2000).
[6] M. Johnsson, K. Törnroos, P. Lemmens, and P. Millet, Chem. Mater. **15**, 68 (2003).
[7] M. Pregelj, O. Zaharko, A. Günther, A. Loidl, V. Tsurkan, and S. Guerrero, Phys. Rev. B **86**, 144409 (2012).
[8] P. Millet, B. Bastide, V. Pashchenko, S. Gnatchenko, V. Gapon, Y. Ksari, and A. Stepanov, J. Mater. Chem. **11**, 1152 (2001).
[9] Z. Wang, M. Schmidt, Y. Goncharov, V. Tsurkan, H.-A. Krug von Nidda, A. Loidl, and J. Deisenhofer, Phys. Rev. B **86**, 174411 (2012).
[10] K. H. Miller, P. W. Stephens, C. Martin, E. Constable, R. A. Lewis, H. Berger, G. L. Carr, and D. B. Tanner, Phys. Rev. B **86**, 174104 (2012).
[11] I. Rousochatzakis, J. Richter, R. Zinke, and A. A. Tsirlin, Phys. Rev. B **91**, 024416 (2015).
[12] M. Pregelj, O. Zaharko, A. Zorko, M. Gomilšek, O. Sendetskyi, A. Günther, M. Ozerov, S. A. Zvyagin, H. Luetkens, C. Baines, V. Tsurkan, and A. Loidl, Adv. Funct. Mater. **25**, 3634 (2015).
[13] A. Zorko, M. Gomilšek, M. Pregelj, M. Ozerov, S. A. Zvyagin, A. Ozarowski, V. Tsurkan, A. Loidl, and O. Zaharko, AIP Adv. **6**, 056210 (2016).
[14] W. Kohn and L. J. Sham, Phys. Rev. **140**, A1133 (1965).
[15] P. E. Blochl, Phys. Rev. B **50**, 17953 (1994).
[16] G. Kresse and J. Hafner, Phys. Rev. B **47**, 558 (1993).
[17] P. Giannozzi, S. Baroni, N. Bonini *et al.*, J. Phys.: Condens. Matter **21**, 395502 (2009).
[18] V. Anisimov, A. Lichtenstein, and F. Aryasetiawan, J. Phys.: Condens. Matter **9**, 767 (1997).
[19] G. H. Wannier, Phys. Rev. **52**, 191 (1937).
[20] V. V. Mazurenko, S. L. Skornyakov, A. V. Kozhevnikov, F. Mila, and V. I. Anisimov, Phys. Rev. B **75**, 224408 (2007).
[21] J. Hubbard, Proc. R. Soc. London, Ser. A **276**, 238 (1963).
[22] A. A. Mostofi, J. R. Yates, Y.-S. Lee, I. Souza, D. Vanderbilt, and N. Marzari, Comput. Phys. Commun. **178**, 685 (2008).
[23] V. V. Mazurenko, S. L. Skornyakov, V. I. Anisimov, and F. Mila, Phys. Rev. B **78**, 195110 (2008).
[24] W. Ku, H. Rosner, W. E. Pickett, and R. T. Scalettar, Phys. Rev. Lett. **89**, 167204 (2002).
[25] O. Janson, I. Rousochatzakis, A. A. Tsirlin, J. Richter, Yu. Skourski, and H. Rosner, Phys. Rev. B **85**, 064404 (2012).
[26] E. Şaşıoglu, C. Friedrich, and S. Blügel, Phys. Rev. B **83**, 121101(R) (2011).
[27] P. Werner, R. Sakuma, F. Nilsson, and F. Aryasetiawan, Phys. Rev. B **91**, 125142 (2015).
[28] I. I. Mazin and D. J. Singh, Phys. Rev. B **56**, 2556 (1997).
[29] D. I. Khomskii, *Transition-Metal Compounds* (Cambridge University Press, Cambridge, UK, 2014).
[30] Toru Moriya, Phys. Rev. **120**, 91 (1960).
[31] P. W. Anderson, Phys. Rev. **115**, 2 (1959).
[32] T. Yildirim, A. B. Harris, Amnon Aharony, and O. Entin-Wohlman, Phys. Rev. B **52**, 10239 (1995).
[33] I. V. Solovyev, J. Phys.: Condens. Matter **20**, 293201 (2008).